Energy and Built Environment 4 (2023) 543–556

Contents lists available at ScienceDirect

Energy and Built Environment

journal homepage: http://www.keaipublishing.com/en/journals/energy-and-built-environment/

Impact of indoor heat load and natural ventilation on thermal comfort of radiant cooling system: An experimental study

K Dharmasastha [a,d,*], D.G. Leo Samuel [b], S.M. Shiva Nagendra [c], M.P. Maiya [a]

[a] Department of Mechanical Engineering, Indian Institute of Technology Madras, Chennai, Tamil Nadu 600036, India
[b] Barghest Building Performance Pte. Ltd., 118 535, Singapore
[c] Department of Civil Engineering, Indian Institute of Technology Madras, Refrigeration and Air Conditioning, Chennai 600036, India
[d] Department of Building Enivironment and Energy Engineering, The Hong Kong Polytechnic University, Hong Kong

ARTICLE INFO

Keywords:
Thermally activated building system
Air-conditioning
Natural ventilation
Thermal comfort
Indoor air quality

ABSTRACT

Construction and operation of buildings are responsible for about 20% of the global energy consumption. The embodied energy of conventional buildings is high due to the utilization of energy-intensive construction materials and traditional construction methodology. Higher operational energy is attributed to the usage of power-consuming conventional air-conditioning systems. Therefore, moving to an energy-efficient cooling technology and eco-friendly building material can lead to significant energy savings and CO_2 emission reduction. In the present study, an energy-efficient thermally activated building system (TABS) is integrated with glass fiber reinforced gypsum (GFRG), an eco-friendly building material. The proposed hybrid system is termed the thermally activated glass fiber reinforced gypsum (TAGFRG) system. This system is not only energy-efficient and eco-friendly but also provides better thermal comfort. An experimental room with a TAGFRG roof is constructed on the premises of the Indian Institute of Technology Madras (IITM), Chennai, located in a tropical wet and dry climate zone. The influence of indoor sensible heat load and the impact of natural ventilation on the thermal comfort of the TAGFRG system are investigated. An increase in internal heat load from 400 to 700 W deteriorates the thermal comfort of the indoor space. This is evident from the increases in operative temperatures from 29.8 to 31.5 °C and the predicted percentage of dissatisfaction from 44.5% to 80.9%. Natural ventilation increases the diurnal fluctuation of indoor air temperature by 1.6 and 1.9 °C for with and without cooling cases, respectively. It reduces the maximum indoor CO_2 concentration from 912 to 393 ppm.

1. Introduction

Climate change poses a major existential threat to life on earth. Fossil energy usage and the associated CO_2 emissions are predominant contributors to climate change. Currently, the building sector accounts for 20% of the world's energy consumption [1]. According to the Intergovernmental Panel on Climate Change [2], reduction in building energy consumption and embodied energy, usage of renewable energy sources, and control of non-CO_2 emissions are the key measures areas to reduce emissions from buildings. Among various electrical appliances, air-conditioners account for a large share of energy consumption [3]. A rapid increase in air-conditioner users, especially in developing countries like India, is expected to consequently increase the energy demand of the air-conditioning sector. In India, air-conditioning of commercial and residential buildings accounts for 32 and 7% of the total building energy consumption, respectively [4]. The embodied energy and the associated embodied CO_2 emission of conventional building materials and traditional construction methodology are significantly high. The United Nations Environment Programme stated that the reduction in building embodied energy would decrease greenhouse gas emissions substantially. Thus, energy-efficient building cooling technology and eco-friendly building material are the need of the hour.

The thermally activated building system (TABS) is a low-carbon substitute for conventional building cooling technology. It can provide better thermal comfort as well as significant energy saving [5]. It can

Abbreviations: GFRG, glass fibre reinforced gypsum; IAQ, indoor air quality; IAT, indoor air temperature (°C); NT, neutral temperature (°C); NV, no ventilation case; NV_WC, No ventilation and with cooling case; OAT, outdoor air temperature (°C); OT, operative temperature (°C); PMV, predicted mean vote; PPD, predicted percentage dissatisfied (%); RCC, reinforced cement concrete; SCC, self compact concrete; TABS, thermally activated building system; TAGFRG, thermally activated glass fibre reinforced gypsum; WC, with cooling case; WV, with ventilation case; WV_NC, with ventilation but no cooling case; WV_WC, with ventilation and with cooling case.

* Corresponding author.
E-mail address: dharmasirkazhi@gmail.com (K. Dharmasastha).

https://doi.org/10.1016/j.enbenv.2022.04.003
Received 31 October 2021; Received in revised form 11 April 2022; Accepted 12 April 2022
Available online 14 April 2022

Nomenclature

B	breadth (m)
C	convective heat loss (W/m^2)
D_R	dry respiration heat loss (W/m^2)
E_d	heat loss by evaporation (W/m^2)
E_s	heat loss by sweating (W/m^2)
H	height (m)
h_c	convective heat transfer coefficient (W/m^2K)
h_r	radiative heat transfer coefficient (W/m^2K)
L	length (m)
L_R	latent respiration heat loss (W/m^2)
M	metabolic rate of body (W/m^2)
Q_{int}	internal heat load (W/m^2)
R	radiation heat loss (W/m^2)
t	thickness (m)
T_a	air temperature (K)
T_{mrt}	mean radiant temperature (K)
T_o	operative temperature (K)
W	width (m)
W	external work done (W/m^2)

reduce energy consumption by 17 (in cool and humid regions) to 42% (in hot and arid regions) compared to the conventional air-conditioning system [6]. It can also be integrated with passive cooling sources such as evaporative cooling and earth tunnel cooling, leading to further energy saving. Glass fibre reinforced gypsum (GFRG) is an eco-friendly building material. It consumes comparatively lesser natural resources, such as water and river sand, for construction. GFRG buildings are suitable for affordable mass housing which is much needed for developing countries like India. The novel combination of TABS and GFRG buildings has a huge energy saving potential and provides a thermally comfortable environment.

The proposed hybrid system is named thermally activated glass fibre reinforced gypsum (TAGFRG), which integrates TABS in GFRG buildings. An experimental room with a TAGFRG roof is constructed within the premises of the Indian Institute of Technology Madras (IITM). The present research paper experimentally investigates the impact of indoor sensible heat load and natural ventilation on the thermal comfort of the TAGFRG system. Thus, it aims to understand the impact of these operating parameters on the system's thermal comfort performance. The outcome of this study could help in optimizing the operating parameters to achieve better comfort at lower energy consumption.

2. Background

2.1. TABS characteristics

TABS is an energy-efficient cooling technology based on the hydronic cooling of building structures. In TABS, the temperature of the interior surfaces of the room is reduced by cooling water circulated through pipes embedded in the room structures. The interior surfaces remove heat from the indoor space and maintain the room in a thermally comfortable condition. The change in working fluid from the air (in the conventional system) to water (in TABS) provides energy saving due to the higher specific heat capacity of water. TABS reduces the peak energy demand by utilizing the thermal mass of the building [6–8]. Radiant cooling systems can only treat the sensible load. Therefore, TABS saves more energy in a hot and dry climate, where the share of the sensible load is higher [9]. Due to the larger heat transfer area, TABS can transfer a vast amount of thermal energy even at a minimal temperature difference. Hence, TABS can provide thermal comfort at a higher supply water temperature, which improves the Coefficient of Performance (COP) of the chiller. The ability of TABS to operate at higher water temperatures makes it suitable for passive cooling systems such as earth tunnel cooling, nocturnal cooling, and evaporative cooling [9–13].

TABS can provide better thermal comfort compared to the conventional air-conditioning system. It eliminates the noise and draft issues [15,16], which are a few major problems with conventional air-conditioning systems. The radiative nature of TABS also helps to provide better thermal comfort. Numerous surveys have found that more than 95% of the occupants feel satisfied with the thermal environment provided by TABS [14]. A field measurement conducted for a study on TABS found that the average Predicted Mean Vote (PMV) was -0.32 and -0.52, and the average Predicted Percentage Dissatisfied (PPD) was 10.1 and 15.6%, for winter and summer, respectively [15]. These PMV and PPD values are well within the recommended comfort limits.

The major limitation of TABS is its inability to treat latent heat, i.e., TABS cannot remove humidity. Hence, the low-temperature cooling surfaces may cause condensation, especially in humid climates. Several strategies were proven to eliminate the condensation risk in TABS. Maintaining the supply water temperature above dew point temperature [16,17] and supplying water above a particular pre-set temperature (say 16 °C) [18,19] are two such strategies. The integration of the radiant and desiccant systems for cooling and dehumidification applications is an energy-efficient combination to avoid the risk of condensation [20]. Membrane assisted radiant cooling system achieved the coldest mean radiant temperature (MRT) of 19.9 °C without any condensation even when the dew point temperature was 23.5 °C [21,22]. TABS responds slower to a change in operating conditions. Therefore, controlling the TABS system is quite challenging [8,23,24]. Moreover, TABS cannot handle sudden indoor load variation. Indoor comfort conditions and condensation on the surfaces limit the surface temperature of TABS to above dew-point temperature, limiting the cooling capacity per unit area.

2.2. Glass fibre reinforced gypsum

GFRG is an alternative building material that is a composite material made of gypsum reinforced with glass fibre. Gypsum is an industrial wastage from the fertilizer industry. Buildings constructed with GFRG panels conserve natural resources by utilizing a minimal quantity of sand, cement, steel, and water. Therefore, GFRG is considered as an eco-friendly and environmentally sustainable building material. GFRG panels are lightweight and thin but strong. The additional advantages of GFRG are its good fire and water-resistant properties [25]. GFRG panel is a preferred building material for rapid construction and is suitable for mass construction. The air cavities in the panel act as a thermal barrier and reduce solar heat penetration [26]. This is extremely important in tropical regions where the conventional reinforced cement concrete (RCC) roof is responsible for 40 to 75% of external heat penetration into the building [27]. The research works on the GFRG panel show that the panels filled with reinforced concrete have sufficient strength to act as load-bearing elements [28,29].

2.3. Internal heat gain

Numerous studies have pointed out the importance of reducing the internal heat gain in a conditioned space. Romani et al. experimentally investigated the performance of radiant walls coupled with a ground heat exchanger for scheduled internal heat gains. They found that the internal heat gain changed the cooling load substantially [30]. Another study found that in a well-insulated building, internal heat gains had a significant impact on the cooling load compared to outdoor conditions [31]. The effect of switching off the lights when not in use was simulated for a typical office building in a moderate climatic region. The floor of the building was equipped with TABS. The study reported an 8% reduction in cooling demand, which resulted in an 18% reduction of the average time for which the Indoor Air Temperature (IAT) exceeded 25 °C.

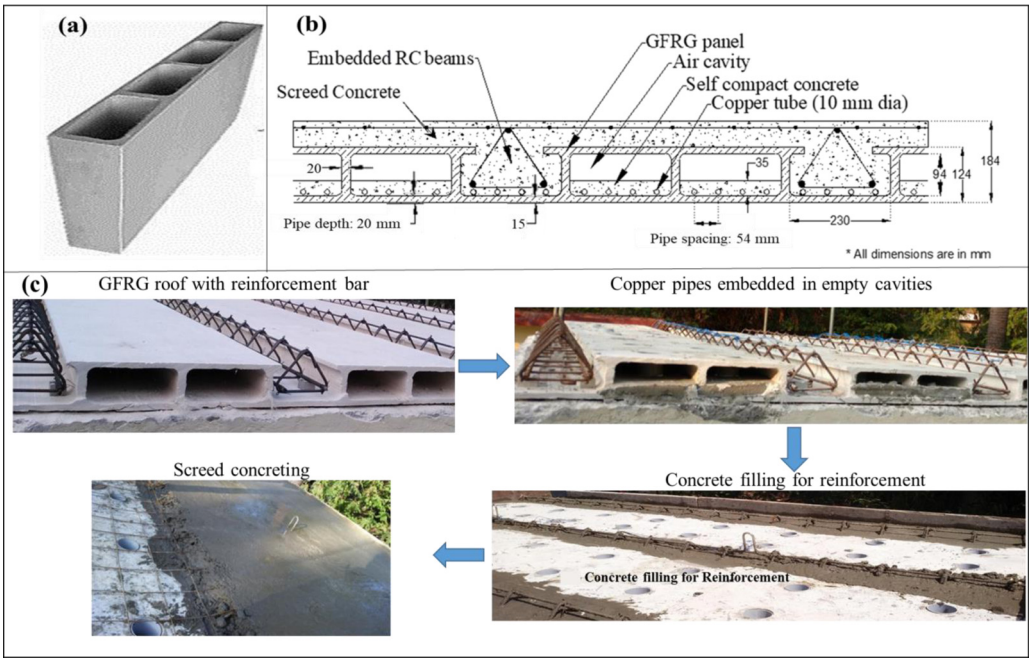

Fig. 1. (a) GFRF Panel (b) Schematic of a cross-section of TAGFRG roof (c) Construction procedure of TAGFRG roof [39].

Table 1
Piping configuration of TAGFRG roof.

SI. No.	Description	Specification
2	Pipe inner diameter	0.01 m
3	Pipe wall thickness	0.001 m
4	Pipe spacing	0.055 m
6	No. of row per cavity	4
7	Pipe length embedded per cavity	12 m
8	Total length of pipe in air-cavities	96 m
9	Total length of pipe in reinforcements	60 m

Thus, switching off lights reduces both lighting and cooling energy usage [32]. Nevertheless, research studies on the influence of internal heat gain on the thermal comfort of TABS are scarce in the literature.

2.4. Natural ventilation

Natural ventilation in a building improves indoor environment quality. In favorable climatic conditions, it also improves the thermal comfort of occupants, and it is an effective passive cooling technology. In a climatic zone with a high fluctuation of diurnal temperature, scheduled ventilation is preferred [33]. Night-time ventilation cools the thermal mass of the building. It reduces and delays the peak and average IAT on the following day. High thermal mass building with good thermal insulation support scheduled natural ventilation [10]. The use of low thermal mass building materials and large window openings will improve the evening thermal comfort level by enhancing the cooling rate. Among ventilation mode, window to wall ratio, window opening type, and floor area, the ventilation mode design feature has the most significant influence on natural ventilation performance [34]. For better ventilation, cross ventilation is preferred over single side ventilation [35]. Natural ventilation dilutes the CO_2 concentration in the indoor space and significantly improves Indoor Air Quality (IAQ).

There are numerous studies on TABS with a mechanical ventilation system. But analyses of TABS with natural ventilation are seldom found in the literature. Leo Samuel et al. [36] experimentally investigated TABS coupled with a cooling tower in the tropical climate of Chennai. They found that scheduled ventilation improved the thermal comfort of TABS in warm and humid regions. Nevertheless, natural ventilation advances the extrema of all indoor comfort parameters by 1.5 h and increases indoor temperature fluctuation, which is undesirable. Taeyeon et al. [37] reported that in a radiant cooled office building with natural ventilation, MRT and operative temperature (OT) were lower than those of the all-air system for the same amount of cooling load. Natural ventilation in a humid climate could cause condensation problems. To ensure a condensation-free radiant cooled surface, its temperature needs to be maintained higher than the dew point temperature of the indoor air. In the present study, the supply water temperature is maintained above 18 °C to avoid condensation problems.

3. Methodology

3.1. Thermally activated glass fibre reinforced gypsum roof

In the TAGFRG roof (Fig. 1), copper pipes are embedded in the GFRG panel cavities. The design parameters of piping are chosen based on the parametric study investigated using numerical simulation [38]. The piping configuration is given in Table 1. Smaller diameter pipes with less pipe spacing are used to have a higher heat transfer area and better cooling performance. Lower pipe spacing allows the pipes to be embedded at the bottom of the cavity (Fig. 1b) without significant non-uniformity of the roof's interior surface temperature. The connection between the reinforcement and the air cavity zones is shown in Fig. 2. This pipe configuration provided a uniform distribution of the roof's interior surface [39]. The construction procedure of the TAGFRG roof is illustrated in Fig. 1C. The TAGFRG roof has reinforcement at every three cavities. In the cavities without reinforcement, i.e., air cavities, the top half is not filled with concrete to utilize the thermal insulating characteristics of air. To achieve this, the concrete used must have high fluidity so that it can flow through the hollow space. Usage of traditional concrete for this application needs vibration, which can damage the panel and the cooling water piping. Hence, a special kind of concrete called Self-Compact Concrete (SCC) that has high flowability is used. The SCC is prepared by adding chemical and mineral admixtures that modify the proportion of the concrete. Superplasticizers, mineral fillers, and viscosity modifying agents are used to increase the fluidity and easy flow of concrete. SCC self-levels without any air void. It is stable and there is no segregation

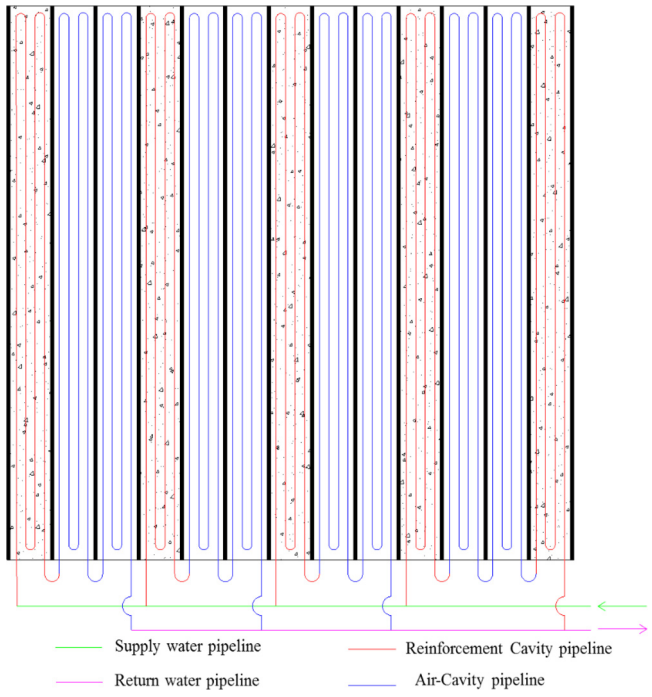

Fig. 2. Piping connection configuration of TAGFRG roof [39].

of components when the concrete is poured. SCC does not compromise the strength and durability of the concrete structure. The spreading diameter of the SCC used for the TAGFRG roof construction is found to be 400 cm using the slump flow test, which is a test used to assess the flowability of concrete. For traditional concrete, high flowability is not desired. Hence, the slump test is used to measure the height of traditional concrete.

3.2. System description

The experimental room (Fig. 3) of dimensions 3.46 m (L) × 3.46 m (B) × 3.15 m (H) is constructed in the premises of IITM, Chennai (13°N, 80°E). Chennai is located on the coast of the Bay of Bengal. It experiences warm and humid weather for most of the year and is classified as a tropical savanna climate or tropical wet and dry climate, according to the Köppen climate classification. This study aims to determine the performance of the cooling system in real-world as well as worst-case conditions. Hence, the experimental facility is constructed in an outdoor environment, i.e., the exterior surfaces of the room investigated are not in a controlled environment. Both the north and south walls of the experimental room have a glazed window each. The room has a partially glazed door on the west wall. The glass used for the windows and door is transparent and 5.5 mm thick. The walls and floor are constructed using conventional building materials, such as bricks for the walls and cement concrete for the floor.

A water chiller of 2 TR capacity with an inbuilt pump is used to circulate the cooling water through the pipes embedded in the TAGFRG roof. The pipes exposed to the outdoor environment are insulated using nitrile rubber. The cooling water temperature is controlled by the electronic thermostat of the water chiller. A manual control valve is used to regulate the water flow rate.

3.3. Monitoring

Temperature and relative humidity of indoor and outdoor air, the temperature of the interior and exterior surfaces of the room, and cooling water temperature are continuously monitored. A data acquisition system is used to record data at one-minute time intervals. In total, temperatures are measured at 68 locations using calibrated T-type thermocouples (copper and constantan). Fig. 4 shows the position of thermocouples used to measure the temperature of different surfaces and indoor air. ASHRAE 55 [40] recommends temperature measurements at heights of 0.1, 0.6, and 1.1 m for a sitting occupant and 0.1, 1.1, and 1.7 m for a standing occupant. In the present study, air temperatures are measured at heights of 0.1, 0.6, 1.1, and 1.7 m. The flow rate of the cooling water does not vary continuously. Hence, it is recorded manually. Indoor CO_2 concentration is measured at one-minute time intervals for the analysis of natural ventilation. The details of the instruments used for the measurements are listed in Table 2.

3.4. Post data analysis

The thermal performance of the present study is quantified in terms of thermal comfort indices. Several factors influence thermal comfort. The most influential factors are IAT, relative humidity, MRT, clothing, and metabolic rate. There are several thermal comfort indices developed to quantify thermal comfort. Among these indices, Fanger's and the adaptive thermal comfort models are widely used [40]. ASHRAE 55 and EN 16798-1 thermal comfort standards have recognized these two

Fig. 3. Experimentation room with TABS.

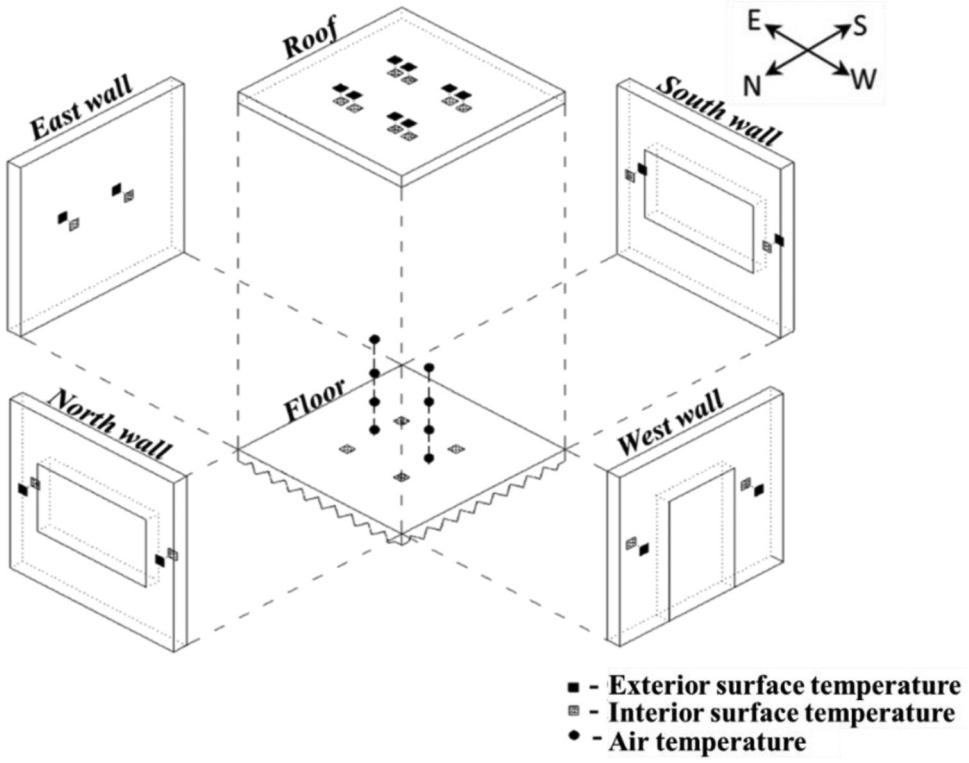

Fig. 4. Measurement locations of surface and air temperatures in the exploded view of the experiment room.

Table 2
Specification of instruments used for monitoring thermal comfort parameters.

Sl. No.	Parameter	Instrument	Make-Model	Measurement Range	Accuracy
1.	Temperature	T-typeThermocouple	-	-200 to 350 °C	±0.5 °C
2.	RH	Hygrometer	Kimo-HM110	5–95 %	±2%
3.	Air velocity	Hot-wire Anemometer	Kimo-CTV110	0 to 5 m/s	±(0.05 m/s + 3%)
4.	Water flow rate	Rotameter	Instrumentation Engg.	219.8 to 2198 LPH58.8 to 588 LPH	±2%
5.	Carbon dioxide	IAQ Meter	TSI - IAQ CALC 7545	0–5000 ppm	±50 ppm or ±3%

models. These two models have specific applications. The details and the suitability of these models for the present study are explained below.

Fanger model quantifies thermal comfort in terms of the PMV and PPD. Tian and Love [15] investigated the thermal sensation of occupants in a space cooled with radiant slab cooling and found that the outcome of their questionnaire survey is consistent with the Fanger model. Several radiant cooling studies available in literature have employed Fanger's model [36,41,42]. The equations (1 and 2) used in Fanger thermal comfort model are given below,

$$PMV = \left[0.303 \times \exp(-0.036M) + 0.028\right] \times \left[M - W - E_d - E_s - L_R - D_R - R - C\right] \quad (1)$$

$$PPD = 100 - 95 \times \exp\left[-0.00353PMV^4 + 0.2179PMV_2\right](\%) \quad (2)$$

Where, M is the metabolic rate of the body (W/m^2), W is the external work done (W/m^2), E_d is the heat loss by evaporation (W/m^2), E_s is the heat loss by sweating (W/m^2), L_R is the latent respiration heat loss (W/m^2), D_R is the dry respiration heat loss (W/m^2), R is the radiation heat loss (W/m^2), C is the convective heat loss (W/m^2).

In the present study, the metabolic rate, clothing resistance, and external work are taken as 1.1 met, i.e., the occupant is assumed to engage in light work, 0.6 clo, i.e., light typical summer clothing and 0 W, respectively. The air temperature, surface temperatures used to calculate MRT, and relative humidity are measured during experimentation.

The OT (T_o) is used to quantify thermal comfort as per the adaptive thermal comfort model. For this model, the OT bands of NT±2.5 °C and NT±3.5 °C provide thermal comfort for 90 and 80% of occupants, respectively, where NT (t_a,°C) is the neutral temperature (NT). NT is the OT at which an average person feels neutral with the thermal environment. It is a function of the outdoor air temperature (OAT) of previous days. The OT and NT are calculated using the below equations (3 and 4) [43].

$$T_o = \left(h_r T_{mrt} + h_c T_a\right)/\left(h_r + h_c\right) \quad (3)$$

$$t_n = 0.31 t_{rm} + 17.8 \quad (4)$$

Where, T_o is the operative temperature (K), h_r is the radiative heat transfer coefficient (W/m^{2}K), T_{mrt} is the mean radiant temperature (K), h_c is the convective heat transfer coefficient (W/m^{2}K) and T_a is the air temperature (K), t_{rm} is the exponentially weighted running mean temperature of outdoor air for the previous days (°C). The convective and radiative heat transfer coefficients are calculated using the method proposed by Causone et al. [44]. They are 4.0 and 6.1 W/m^{2}K, respectively (Appendix B).

Adaptive thermal comfort models were developed for naturally ventilated buildings. However, recent studies suggested that the adaptive thermal comfort model can be used for conditioned buildings if the occupants can control the cooling [45]. Hence, in recent years, the adaptive thermal comfort model is also used for conditioned spaces [36,46].

Table 3
Extrema and average thermal comfort parameters for various cases of internal heat loads.

SI. No.	Parameters		Internal heat load			
			400 W(44.4 W/m^2)	500 W(55.5 W/m^2)	600 W(66.6 W/m^2)	700 W(77.7 W/m^2)
1	OAT, °C	Minimum	27.5	27.5	28.3	27.8
		Average	30.9	30.8	31.1	31.0
		Maximum	36.9	36.2	36.4	36.9
2	IAT, °C	Minimum	29.1	30.0	29.8	30.9
		Average	29.9	30.6	30.4	31.7
		Maximum	31.1	31.3	31.0	32.9
3	MRT, °C	Minimum	29.1	29.6	29.8	30.1
		Average	29.7	30.1	30.4	30.8
		Maximum	30.2	30.6	31.0	31.4
4	PMV, -	Minimum	1.1	1.4	1.6	1.8
		Average	1.4	1.7	1.9	2.1
		Maximum	1.8	1.9	2.4	2.6
5	PPD, %	Minimum	28.7	46.5	53.8	65.2
		Average	44.5	59.1	69.6	80.8
		Maximum	68.2	73.0	90.6	95.1
6	OT, °C	Minimum	29.1	29.9	30.2	30.7
		Average	29.8	30.5	30.9	31.5
		Maximum	30.8	31.0	31.9	32.4
7	80% adaptive comfort band, °C	Lower limit	22.9	22.7	22.9	22.9
		Neutral	26.4	26.2	26.4	26.4
		Upper Limit	29.9	29.7	29.9	29.9

4. Results and discussion

The influences of the internal heat load and natural ventilation on the thermal performance of the TAGFRG roof are analyzed. The performance is quantified in terms of the thermal comfort parameters, namely, IAT, MRT, PMV, PPD, and OT.

4.1. Internal heat load

The monitoring system consists of a data acquisition system, computer, 24 V DC supply for humidity transmitters, hot wire anemometers, PMV-PPD index meter, and a desktop. It consumes about 400 W of energy. This energy is taken as the base internal heat load. The internal heat load is increased from this base level to 700 W with an interval of 100 W using 100 W incandescent light bulbs. One bulb is switched on for every 100 W increase in the internal heat load investigated. The internal heat load is constant throughout each experiment. The 100 W considered is approximately equal to the heat emitted by a human at rest [47]. As per the ASHRAE 55 standard, the average height of a sitting human is 1.1 m. A few studies in the literature have considered this height to replicate the human heat source [40,48,49]. Hence, the incandescent bulbs are placed at a height of 1.1 m to replicate the heat source of an occupant sitting in the centre of the room. Ventilation and fenestration could vary significantly among different internal heat load cases. To minimize the influence of these variables, windows are closed, and their glasses are covered with insulation. Cooling water is supplied to the TAGFRG roof at a flow rate of 600 lph and a temperature of 20 °C. For each condition, the experiment setup is run continuously for two days. The second day's data is used in this analysis to reduce the influence of heat storage on the thermal mass of the building during the previous operating condition. The experiments are conducted during hot summer days to evaluate the thermal comfort performance in worst-case conditions. Table 3 presents the extrema and average thermal comfort parameters for different internal heat load cases.

4.1.1. Outdoor conditions

It is vital to know the outdoor conditions during experimentation as they influence indoor thermal comfort. The differences in OAT between the cases studied are minimal. The solar radiation data is obtained from a continuous ambient air quality monitoring station located beside the experiment room. The differences in solar radiation intensity between the cases studied are insignificant except from 12:00 to 16:00 h (Fig. 5). In this period, the OAT is highest for the 700 W case and lowest for the 500 W case. During the entire study duration, the OAT varies from 27.5 to 36.9 °C. The diurnal temperature fluctuations for 400, 500, 600, and 700 W cases are 9.4, 8.7, 8.4, and 9.1 °C, respectively. As the study is conducted in April, i.e., summer, the diurnal average temperatures are above 30 °C, and the maximum temperatures are above 36 °C for all the cases.

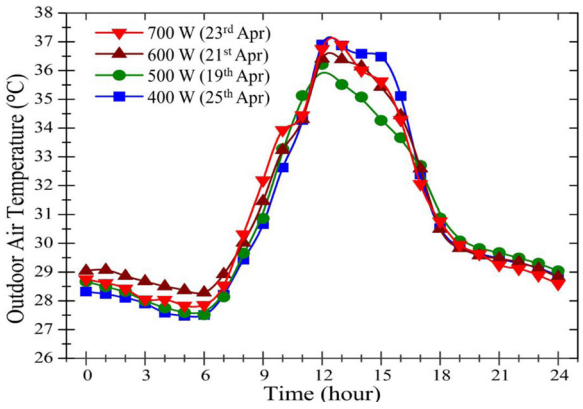

Fig. 5. Diurnal variation of OAT on the days the effect of internal heat loads were investigated.

4.1.2. Indoor air temperature

The internal heat load heats the surrounding air by convection. Hence, it has a notable influence on IAT. An increase in heat load from 400 to 700 W increases the average IAT from 29.9 to 31.7 °C. The diurnal profile of IAT for the 500 W case is slightly different from the rest (Fig. 6) due to the sudden fall in OAT at noon. Excluding the 500 W case, the diurnal profile of IAT for the remaining cases is similar. The thermal mass of the structure has no considerable influence on the heat transfer between the internal load and the indoor air. Hence, the thermal lag between peak IAT and OAT is almost the same for all the cases. The peak temperatures of all cases are attained at the same time, i.e., 16:00 h. The diurnal fluctuation of IAT is much lower than that of OAT.

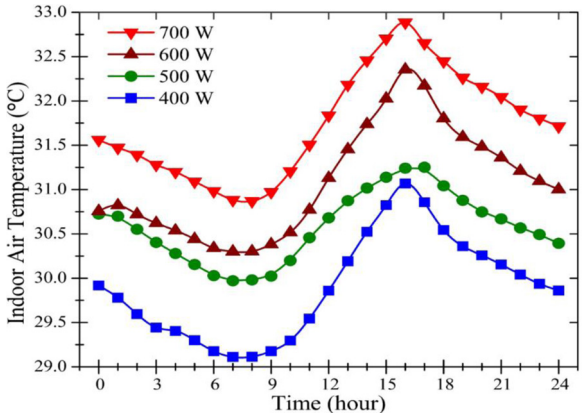

Fig. 6. Diurnal variation of IAT for various internal heat loads.

Even though OAT fluctuates by 8.1 to 9.4 °C, diurnal fluctuation of IAT is less than 2 °C. IAT and OAT have a considerable time lag. The lower fluctuation of IAT and time lag between IAT and OAT are due to the thermal mass of the building.

A high vertical temperature gradient can affect thermal comfort. For the 400 W case, the vertical temperature gradient is lower than that of other cases (Fig. 7). The vertical temperature gradient increases with the increase in heat load. For all the cases, the IAT at 0.6 m height is higher than that of other vertical locations as the heat source is near this height. Relatively warm air at 0.6 m height moves up due to buoyancy and is cooled by the TAGFRG roof and air mixing. The resulting air movement counteracts the vertical temperature gradient. For all the cases, the differences in IAT between the head and ankle levels for both sitting (0.1 and 1.1 m) and standing positions (0.1 and 1.7 m) are less than 1 °C. Thus, the vertical air temperature difference between the head and ankle height levels of all the cases is within the acceptable limit of less than 3 °C prescribed by ASHRAE 55 [40].

4.1.3. Mean radiant temperature

Interior roof surface temperature and MRT are essential to quantify the performance of the TAGFRG roof (Fig. 8). The increase in the internal heat load increases the temperature of the interior roof surface to remove the additional heat load. The average temperature of the interior roof surface for the 400 W case is 24.4 °C, and it increases to 25.1 °C for the 700 W case (Fig. 8b). The internal heat load has a lower influence on the temperature of interior surfaces than that of indoor air. Hence, the difference in average diurnal MRT between the different heat loads investigated is lower than that of the IAT. The average diurnal MRT for the 400 W case is 29.7 °C. It increases by just 0.4 °C for the 700 W case. For the 500 W case, due to the sudden fall in OAT during afternoon hours, the interior roof surface temperature and MRT are lower than those of the other cases during afternoon hours.

4.1.4. Operative temperature

An increase in internal heat load increases the IAT and MRT, which in turn increases the OT (Fig. 9). For the 400 W of heat load, the average diurnal OT is 29.8 °C, and it rises to 30.5, 30.9, and 31.5 °C for 500, 600, and 700 W, respectively. The extrema and average of OT and neutral temperature and its comfort band limits are mentioned in Table 3. As per the ASHRAE 55 adaptive thermal comfort model, the average diurnal OT for 500, 600, and 700 W is outside the 80% adaptive thermal comfort band, i.e., NT ± 3.5 °C all through the day. For the 400 W of internal heat load, the average OT falls within the 80% comfort band. Hence, on average, the room is comfortable if the internal load does not exceed 400 W (44.44 W/m^2).

The running mean outdoor temperature during the experimental study is 27.8 °C. As per the adaptive thermal comfort method of EN 16798-1 [50], the acceptability limits of OT are 25 to 30 °C (Class I), 24 to 31.0 °C (Class II), and 23 to 32 °C (Class III) [51]. For 400 and 500 W cases, the maximum OT is within the Class II range; hence, the room is always thermally comfortable for class II category occupants. Class I is the most restrictive and is for elderly occupants. The internal heat load of 400 W provides a comfortable environment for the Class

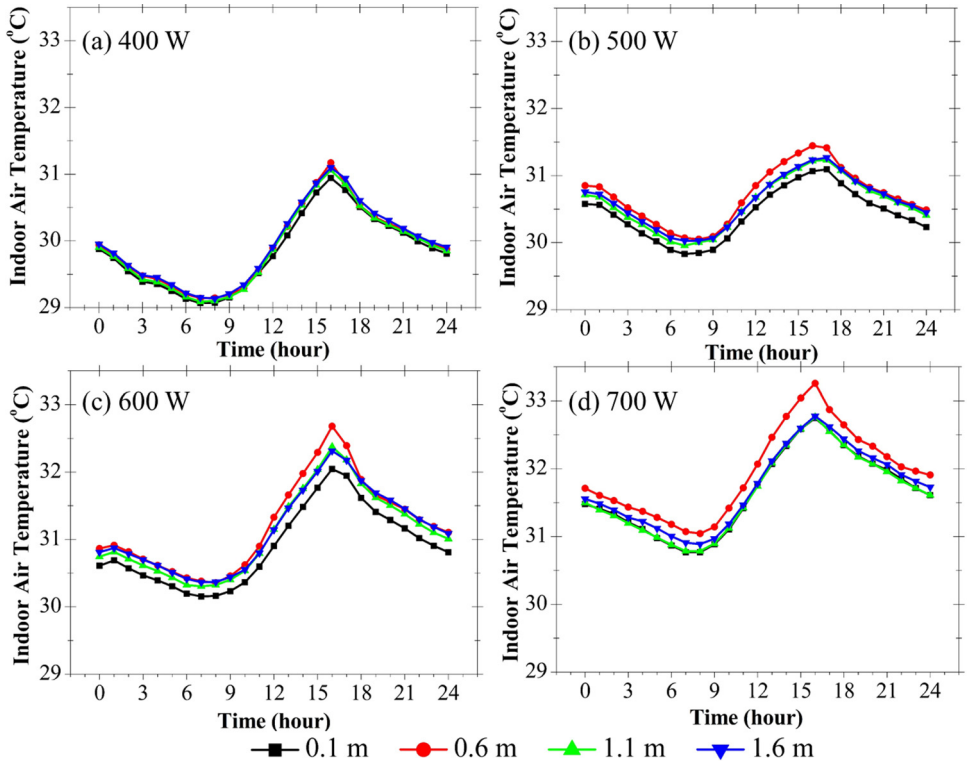

Fig. 7. Diurnal variation of air temperature at different heights for various internal heat loads.

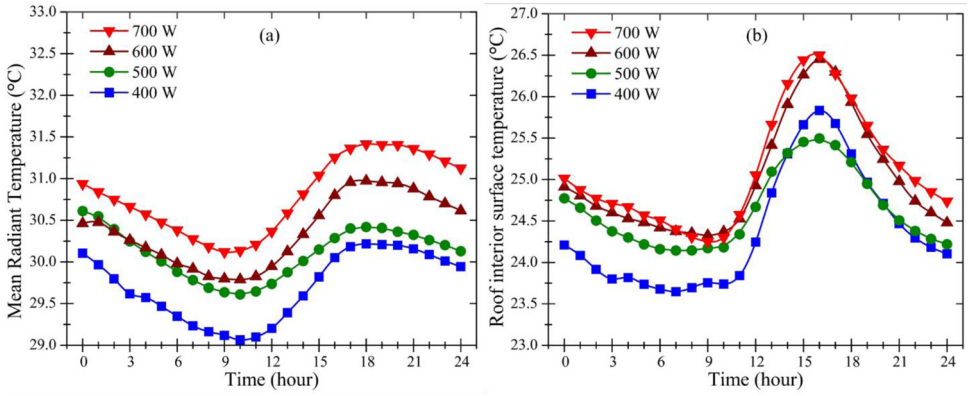

Fig. 8. Diurnal variation of (a) MRT and (b) roof interior surface temperature for various internal heat loads.

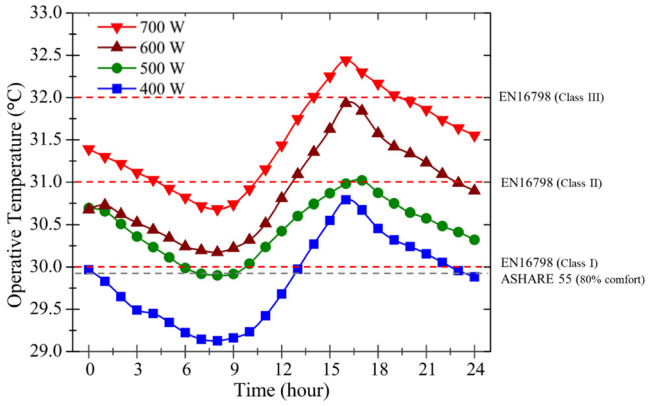

Fig. 9. Diurnal variation of OT for various internal heat loads.

I category occupants between 1:00 and 15:00 h. The internal load of 700 W fails to provide thermal comfort during peak hours, i.e., 14:00 to 19:00 h, even for the class III category occupants. For Class III, the proposed cooling system can handle up to 66.66 W/m^2 (600 W) of internal heat load on a summer day in a warm and humid climate. The proposed system cannot provide a comfortable indoor environment for the Class I category people during peak hours, even with the minimum cooling load of 400 W investigated in this study. The lower heat transfer rate is due to relatively higher water temperature to avoid condensation issues in the humid climate. The proposed system must be integrated with a dehumidification system to increase the cooling capacity per unit area without condensation issues. When coupled with a dehumidification system, the cooling capacity of the proposed system can be increased by reducing the cooling water temperature.

4.1.5. *Predicted mean vote & predicted percentage dissatisfied*

Compared to the adaptive thermal comfort model, the Fanger model is stringent. For all the cases, the PMV is always higher than +1 (Fig. 10a), which is not desirable. An increase in internal heat load increases PMV. The average PMV for 400 W is 1.4, and it rises to 1.7, 1.9, and 2.1 for 500, 600, and 700 W, respectively. Thus, an increase in internal load makes the indoor space more uncomfortable. For all the cases investigated, the PMV value is lowest at around 8:00 h and highest at around 16:00 h.

The average diurnal PPD for the 400 W case is 45%, which increases to 59%, 70%, and 81% for 500, 600, and 700 W cases, respectively (Fig. 10b). For the 400 W case, less than 50% of people are dissatisfied from midnight to noon, as the thermal mass delays the increase in temperature. Around 16:00 h, PPD attains the peak for all the cases. An increase in internal heat load from 400 to 700 W increases the peak PPD by 27%. The lowest PPD observed in the study (28%) is far from the acceptable range. As per Fanger's model / the Fanger model, the proposed system cannot provide acceptable thermal comfort all the time, even for the existing heat load, i.e., 400 W.

4.2. *Natural ventilation*

The influence of natural ventilation on the thermal comfort of the TAGFRG roof is investigated. Three different experimental cases are studied, namely No Ventilation but With Cooling (NV_WC), With Ventilation and With Cooling (WV_WC), and With Ventilation but No Cooling (WV_NC). For the With Cooling (WC) cases, the cooling water to

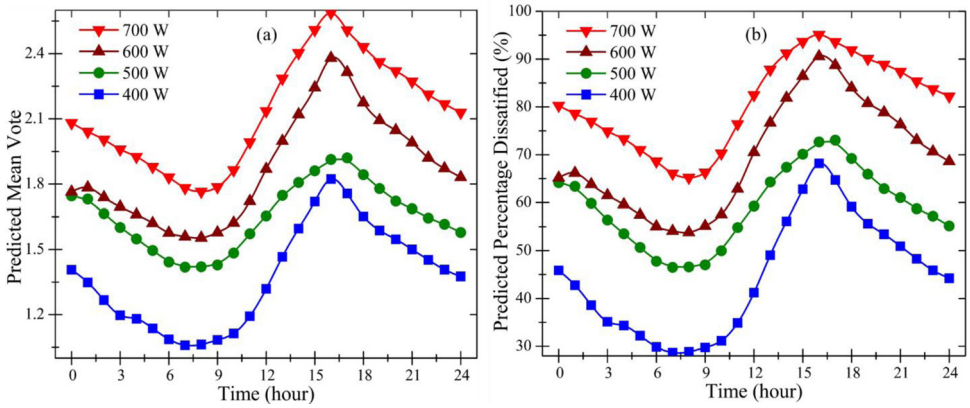

Fig. 10. Diurnal variation of (a) PMV and (b) PPD for various internal heat loads.

Table 4
Extrema and average of the thermal comfort parameter for various cases of ventilation.

SI. No.	Parameters		No ventilation _ With Cooling (NV_WC)	With Ventilation _With Cooling (WV_WC)	With Ventilation _No Cooling (WV_NC)
1	OAT, °C	Minimum	27.5	27.7	28.4
		Average	30.9	31.0	31.5
		Maximum	36.9	37.0	37.1
2	IAT, °C	Minimum	29.1	29.1	30.3
		Average	29.9	30.7	32.0
		Maximum	31.1	32.7	34.2
3	MRT, °C	Minimum	29.1	29.3	31.0
		Average	29.7	30.1	32.2
		Maximum	30.2	30.8	33.5
4	PMV, -	Minimum	1.1	1.1	1.6
		Average	1.4	1.7	2.3
		Maximum	1.8	2.4	3.1
5	PPD, %	Minimum	28.7	32.1	58.5
		Average	44.5	61.1	83.7
		Maximum	68.2	92.3	99.4
6	OT, °C	Minimum	29.1	29.2	30.5
		Average	29.8	30.5	32.1
		Maximum	30.8	32.1	33.8
7	80% adaptive comfort band, °C	Lower limit	22.9	22.9	22.9
		Neutral	26.4	26.4	26.4
		Upper Limit	29.9	29.9	29.9

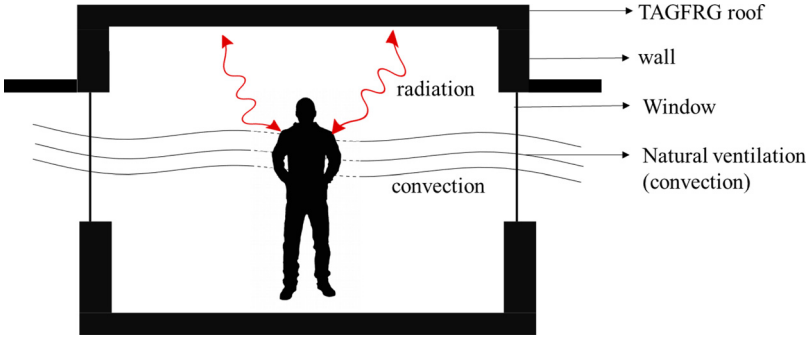

Fig. 11. Section view of TAGFRG roof system.

the TAGFRG roof is supplied at 20 °C and 600 lph. Table 4 tabulates the extrema and average of OAT and thermal comfort parameters for the cases investigated. In this study, the room is naturally ventilated by opening the windows in the north and south walls, i.e., cross ventilation (Fig. 11). Each window measures 2 m (W) × 1.2 m (H), but only 50% of the window area is openable, i.e., an operable area of 1.2 m^2. In the present investigation, the diurnal average of air velocity measured for the natural ventilation cases is 0.3 m/s, i.e., the average airflow is 0.36 m^3/s.

4.2.1. Outdoor air temperature

The diurnal profiles of OAT on all the experimental days are almost similar (Fig. 12a). A low OAT variation between the cases will provide a better understanding of the influence of ventilation. The peak OAT varies from 36.9 to 37.1 °C, while the average OAT fluctuates between 30.9 and 31.5 °C (Table 4). Even a marginal change in outdoor conditions is accounted for while discussing thermal comfort parameters.

4.2.2. Indoor air temperature

The average IAT is 32 °C if the room is ventilated but not cooled. Cooling with TAGFRG reduces the average IAT by 1.3 °C. In the WV_WC case, the IAT is higher than the OAT most of the day. Hence, the fresh air coming into the indoor space increases the cooling demand of the room. Thus, restricting natural ventilation is expected to improve indoor comfort parameters. This is evident from the reduction in the average IAT by 0.8 °C for the NV_WC compared to the WV_WC case. Ventilation advances the peak IAT. The peak temperature for the NV_WC case is attained at 16:25 h; it advances to 15:10 h for the WV_WC case (Fig. 12b). Ventilation also increases the diurnal fluctuation of IAT. Among the WC cases, ventilation increases the diurnal fluctuation of IAT by 1.6 °C. From 0:00 to 7:00 h, there is a very minimal difference in IAT between WV_WC and NV_WC cases due to lower wind speed and lower temperature difference between OAT and IAT during that period. The slightly lower IAT for the WV_WC case is due to the movement of colder outdoor air into the room. Nevertheless, the difference in IAT is minimal, because, in humid tropical climates, the drop in OAT at night is lower compared to that of dry climatic regions.

After 7:00 h, the IAT of the WV_WC case is higher than the NV_WC case as the ventilation by warm outdoor air heats the indoor space. For the WV cases, IAT is higher than OAT during the absence of solar radiation, i.e., 18:00 to 7:00 h, despite a direct interaction between indoor and outdoor air. It is due to the heat load in the indoor space and the heat transfer from the warmer building surface that stores heat during the daytime. When the room is ventilated, the IAT attains the peak almost at the same time, for both cooling (WV_WC) and no cooling (WV_NC) cases. Thus, if the room is ventilated, TAGFRG has no considerable influence on the thermal lag between OAT and IAT.

4.2.3. Mean radiant temperature

Ventilation increases the IAT during the daytime, which in turn increases the interior surface temperatures and MRT (Fig. 13a). The maximum MRT for the NV_WC case is 30.2 °C, which increases to 30.6 °C for the WV_WC case. Ventilation also increases the diurnal fluctuation of MRT. The diurnal fluctuation of the NV_WC case is 1.1 °C, and it in-

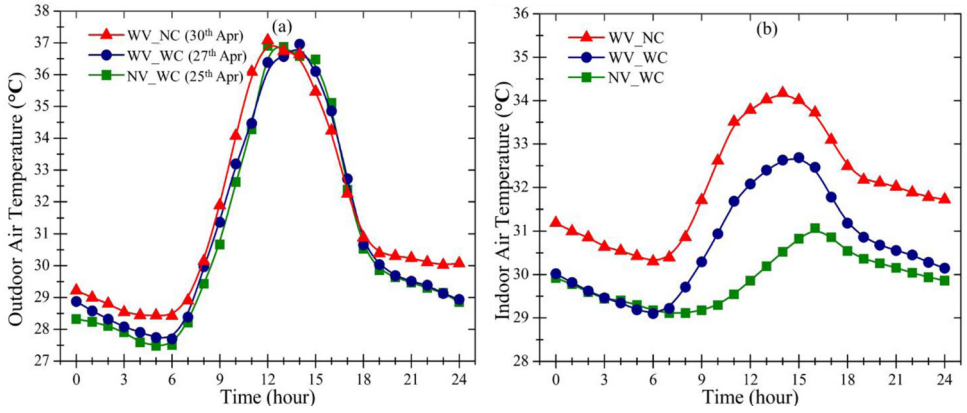

Fig. 12. Diurnal variation of (a) OAT on the days of experiments and (b) IAT for various cases of ventilation.

creases to 1.5 °C for the WV_WC case. The maximum MRT is attained at 18:00 h for the NV_WC case. The time is advanced by 2 h for the WV_WC case. The minimum temperature for the NV_WC case is 29.1 °C and is reached at 10:00 h. It increases to 29.3 °C and the time is advanced to 7:00 h for the WV_WC case. Thus, ventilation advances the time at which the maximum and minimum temperatures are reached. For no ventilation case, the thermal mass of the building retards the temperature for a longer duration. Ventilation increases the rate of heat transfer and thus advances the extrema.

The WV_NC and WV_WC cases are compared to understand the impact of cooling in the presence of ventilation. For these cases, the diurnal profile is almost similar. Both these cases attain maximum and minimum MRT at the exact times. Thus, cooling does not influence the time at which the extrema of MRT are attained, significantly if the building is ventilated and the building cooling is maintained constant. However, cooling (WV_WC) reduces the fluctuation in MRT by 1 °C compared to the WV_NC case.

4.2.4. Operative temperature

Fig. 13b depicts the diurnal variation of OT and the upper limit of 80% comfort band for the various ventilation cases investigated. Ventilation increases the average OT as the IAT and MRT increase due to the influence of warm outdoor air. The average OT for the NV_WC case is 29.8 °C, which increases to 30.5 °C for the WV_WC case. As per the ASHRAE 55 adaptive thermal comfort model, the average OT of NV_WC is within the 80% comfort band limit, i.e., NT±3.5 °C, where NT is 26.4 °C. However, the instantaneous OT of NV_WC is within the 80% comfort band, from 0:00 to 12:00 h. For the WV_WC case, the indoor space is within 80% comfort for 8 h only. The OT for the WV_NC case is always out of the 80% comfort band. As per EN 16798-1 [50], the NV_WC provides a comfortable environment even for class I category occupants. For the WV_WC case, the OT exceeds the acceptability limit from 14:00 to 16:00 h. The discussion provided in the MRT for the thermal lag is also valid for OT. The thermal lag is influenced significantly by the ventilation but not significantly by cooling.

4.2.5. Predicted mean vote and predicted percentage dissatisfied

Ventilation brings warm outdoor air indoors. Therefore, it increases both IAT and MRT. Hence, as shown in Fig. 14, both PMV and PPD are always more for the cases with ventilation. Among the cooling cases, ventilation increases the average PMV from 1.4 (NV_WC) to 1.7 (WV_WC), and the average PPD increases by 17%. Nevertheless, the influences of ventilation on PMV and PPD are not significant from midnight to 6:00 h because of a lower difference between IAT and OAT during that period. OAT increases after 6:00 h. The warm outdoor air ventilated into the indoor space increases the PMV and PPD rapidly. Between 6:00 and 12:00 h, PPD increases by 53% if the room is cooled and ventilated (WV_WC) but only by 11% if the room is cooled but not ventilated (NV_WC). Eventually, the WV_WC case attains a maximum PPD of 92%, whereas the maximum PPD for the NV_WC case is 68%. High OAT during late evening and early morning hours, resulting from the heat island effect, keeps the PMV and PPD values of WV higher than the NV case. Thus, improperly scheduled natural ventilation will deteriorate thermal comfort in a warm tropical climate.

4.2.6. Indoor CO_2 concentration

Space with poor IAQ will lead to sick building syndrome (SBS). Poor ventilation is a vital contributor to poor IAQ [52,53]. A higher concentration of CO_2 is the prevailing predictor for IAQ, as the concentration of CO_2 correlates well with SBS [54,55]. Higher indoor CO_2 concentrations impact the decision-making ability of the occupants [56]. In this experimental work, the CO_2 concentration is measured at the centre of

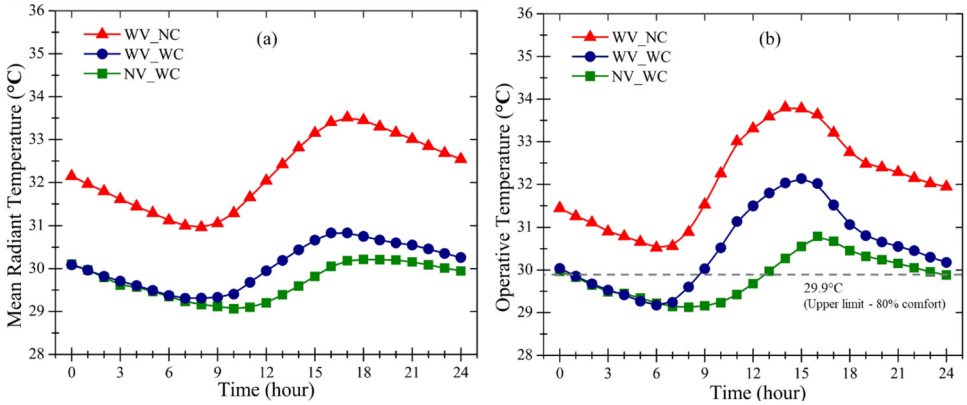

Fig. 13. Diurnal variation of (a) MRT and (b) OT for various cases of ventilation.

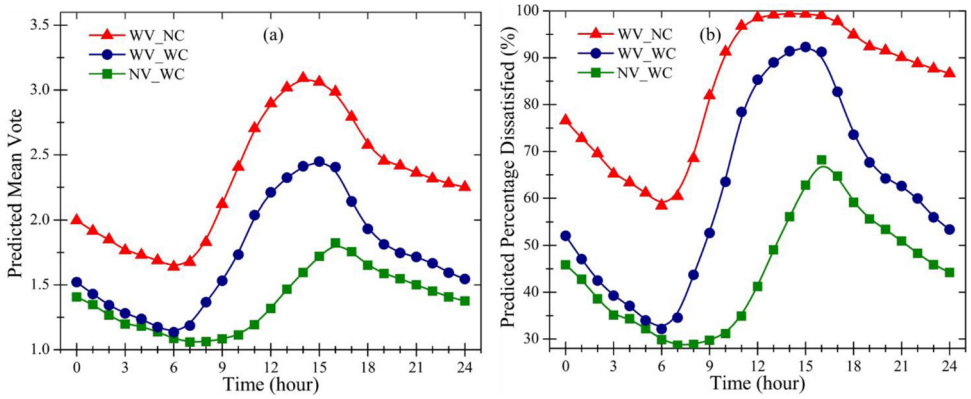

Fig. 14. Diurnal variation of (a) PMV and (b)PPD for various cases of ventilation.

Table 5
Occupation timings.

Cases	No ventilation _ With Cooling (NV_WC)	With Ventilation _With Cooling (WV_WC)
Session 1	10:00–12:40	12:30–17.30
Session 2	13:30–18:00	20:30–21:30

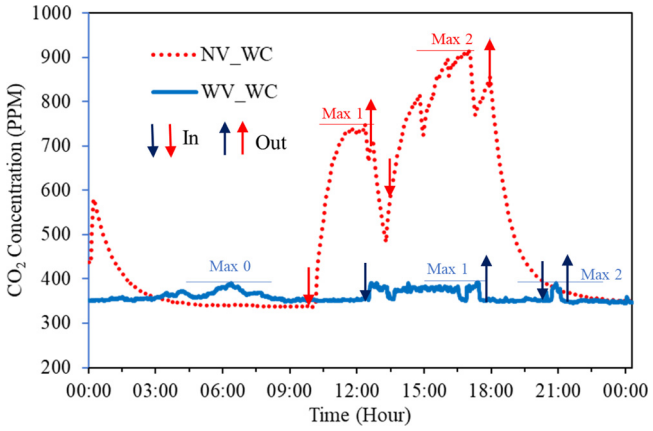

Fig. 15. Indoor variation of CO_2 concentration for various cases of ventilation.

the room, at a height of 1.1 m from the floor surface (assuming the occupant is in a seated position). CO_2 concentration is measured for a single occupant in the room, and the occupation timings are listed in Table 5.

Fig. 15 depicts the diurnal variation of indoor CO_2 concentration for the NV_WC and WV_WC cases. The initial high concentration of NV_WC case at around 00:15 h (580 ppm) is attributed to the previous day's room occupancy to switching on the instruments. During the non-occupational hours, the maximum CO_2 concentration recorded for the NV_WC case is 340 ppm. During occupancy, CO_2 concentration increases to 912 ppm which is within the permissible limit [57]. For the first occupancy hours (Session 1), the time taken to reach the maximum CO_2 concentration, i.e., 750 ppm, is 2 h 20 minutes after the occupant enters the room. For Session 2, after the occupant leaves the room, it takes 3 h for CO_2 concentration to fall to the background level, i.e., 351 ppm.

For the ventilation case, the fluctuation in indoor CO_2 concentration during morning hours could be due to a change in outdoor CO_2 concentration. The experimental facility is located in a reserved forest, and the absence of photosynthesis could have increased the CO_2 concentration till 6:00 h. During occupancy, the maximum CO_2 concentration of the ventilation case is 393 ppm, as the fresh air dilutes the indoor CO_2 concentration. The time taken to reach the saturation level for both occupancy and non-occupancy cases is less than 30 minutes due to the higher movement of outdoor air into the indoor space.

5. Conclusions

The influences of internal heat load and natural ventilation on the thermal comfort of the TAGFRG roof system are investigated experimentally for the climatic conditions of Chennai. The internal heat source is increased from 400 to 700 W with intervals of 100 W for an indoor space of 9 m^2 floor area. The salient conclusions of the study are listed below.

- The average diurnal OT for an internal load of 400 W is 29.8 °C, which increases to 31.5 °C for an internal heat load of 700 W. As per the ASHRAE 55 adaptive thermal comfort model, for 400 W of internal heat load, the indoor space is within 80% thermal comfort limit for 14 h of a day. The remaining cases are always outside the 80% comfort limits. As per the EN-16798 adaptive thermal comfort model, the room offers thermal comfort for Class II and III category occupants when the indoor load does not exceed 500 and 600 W, respectively.
- As per Fanger's thermal comfort model, the predicted percentage of dissatisfied (PPD) is less than 45% for 400 W of internal heat load. For the remaining cases, PPD is greater than 59%.
- The thermal lag between indoor and outdoor temperatures is found to be independent of internal heat gains. In other words, the time of attaining peak indoor temperature is not influenced by the internal load.

Three ventilation cases have been experimentally investigated for this study; they are No Ventilation and With Cooling (NV_WC), With Ventilation and With Cooling (WV_WC), and With Ventilation and No Cooling (WV_NC). The room is naturally ventilated by opening the windows in the north and south walls.

- Ventilation cases reduce the time lag between the peak of indoor and outdoor temperatures. It also increases the diurnal fluctuation of IAT, MRT, and OT.
- Natural ventilation increases the average PPD value from 44.5% for NV_WC to 61.1% for WV_WC, which is undesirable.

Ventilation decreases the maximum CO_2 concentration from 912 to 393 ppm for single occupancy, which in turn improves the IAQ.

Declaration of Competing Interest

The authors declare that they have no known competing financial interests or personal relationships that could have appeared to influence the work reported in this paper.

CRediT authorship contribution statement

K Dharmasastha: Conceptualization, Methodology, Investigation, Writing – original draft, Writing – review & editing. **D.G. Leo Samuel:** Data curation, Writing – review & editing. **S.M. Shiva Nagendra:** Supervision, Writing – review & editing. **M.P. Maiya:** Conceptualization, Resources, Supervision, Writing – review & editing.

Acknowledgment

The authors thank the Department of Science and Technology (DST), Government of India, New Delhi for funding this study (Reference No.: SR/S3/MERC/00091/2012).

Appendices

Appendix A: trendline of thermal comfort indices for heat load variation

The trendline is plotted to find the correlation between thermal comfort indices and internal heat load. The second-order polynomial trendlines are plotted for the diurnal average of each thermal comfort parameter, and the corresponding trendline equations are mentioned in the respective figures (Figs. A.1 to A.4). The extrema of the thermal comfort parameters for each internal heat load case are also plotted. The experimental facility is constructed outdoor, and the study is conducted during summer. Thus, trendline (regression) analysis estimates the maximum permissible internal heat load for the worst-case condition for that location. The trendline equation can estimate the change in thermal comfort parameters for their respective internal heat load conditions. The discussion on the influence of internal heat load provided in the result and discussion section is also valid for the trendline analysis of thermal comfort parameters.

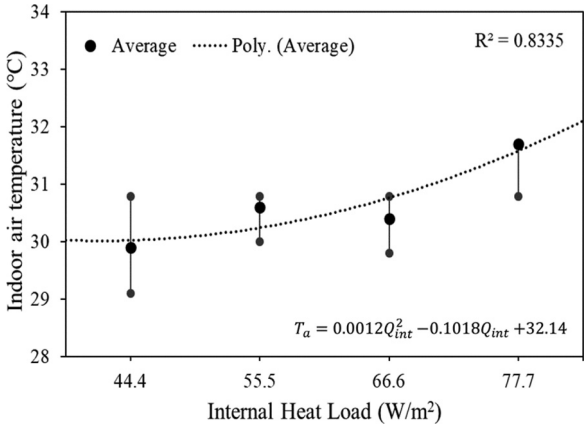

Fig. A.1. Trendline of IAT variation corresponding to the internal heat load.

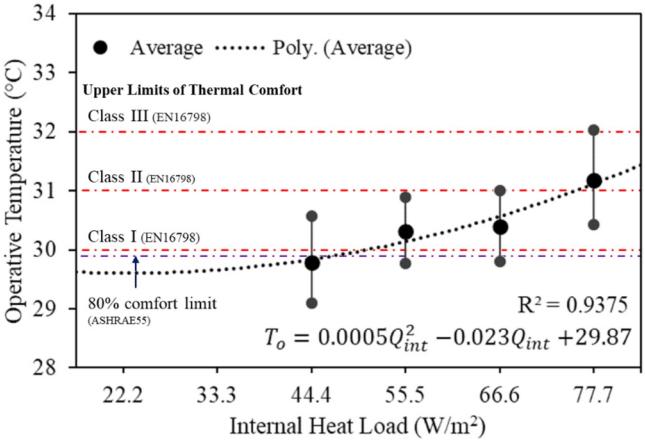

Fig. A.3. Trendline of OT variation corresponding to the internal heat load.

These regression equations are applicable only for similar conditions. The regression is valid if the indoor heat load is in the range of 44.4–77.7 W/m^2 and the building is in a warm and humid climate with the peak outdoor air temperatures from 36.2 to 36.9 °C. The regression equation aids in finalizing the indoor heat load for similar structures and required thermal comfort. In the present study, the roof is exposed to solar radiation. Hence, the proposed regressions apply to buildings' top floors only. For the other floors, the proposed regression equations can overestimate the thermal comfort parameters and can be corrected using correction factors estimated from further studies. The raw data of the research work are stored in a data repository to assist future research in related areas [58].

Figs. A.1 and A.2 depict the trendline of diurnal average IAT, interior roof surface temperature, and MRT for various internal heat loads investigated. The IAT trendline reveals a strong positive correlation between IAT and internal heat load, as the heat load directly warms up the indoor space. The trendline slope of MRT and interior roof surface temperatures are comparatively less than that of IAT, i.e., the influence of internal heat load on the MRT and the radiant cooling surface is not as significant as that on the IAT. The R^2 values of the obtained trendline are 0.83 and 0.99 for IAT and MRT respectively. It indicates that the obtained trendlines have a better fit with the experimental results.

The trendlines for the thermal comfort indices, i.e., OT, PMV and PPD, are shown in Figs. A.3 and A.4. The R^2 values of the obtained PMV-PPD and OT trendlines are 0.9, i.e., best match with the experimental

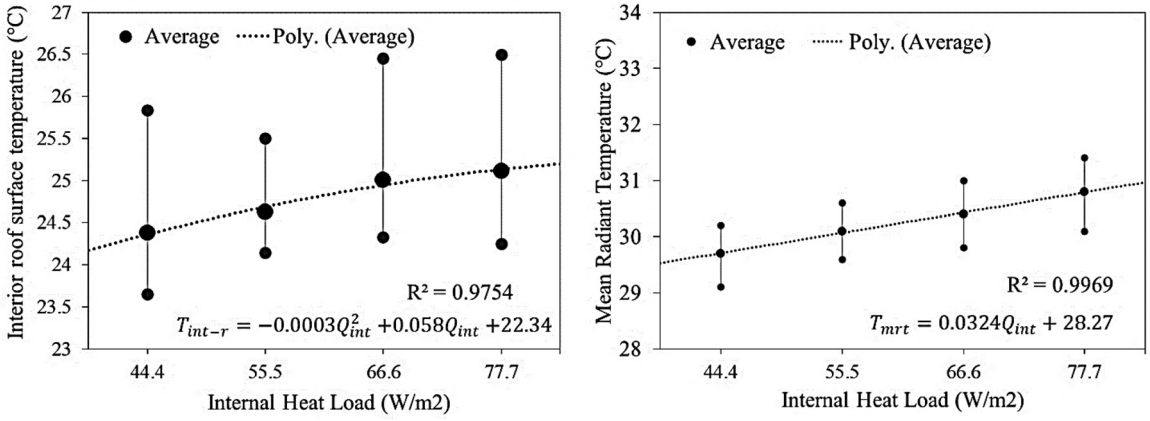

Fig. A.2. Trendline of (a) Interior roof surface temperature (B) MRT variation corresponding to the internal heat loads.

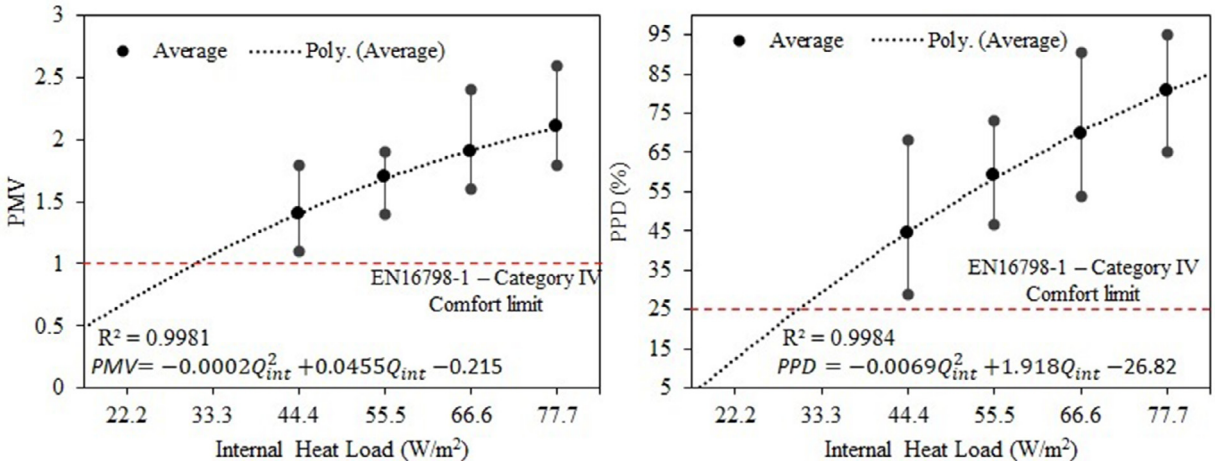

Fig. A.4. Trendline of (a) PMV (b)PPD variation corresponding to the internal heat load.

results. The upper comfort limits of the adaptive thermal comfort model of ASHRAE 55 and EN 16798-1 are indicated in Fig A.3. The extrapolation of the trendline towards the lower internal heat loads reveals that the internal heat loads of 400 W, i.e., 44.44 W/m^2 and lower provide thermal comfort with diurnal average OT complying with 80% acceptability limit of ASHRAE 55 and Class I category of EN 16798-1. As per Fanger's thermal comfort model, the PMV and PPD trendlines show that internal heat loads lesser than 22.2 W/m^2 can provide a comfortable environment [50].

Appendix B: heat transfer coefficient calculation

The convective and radiative heat transfer coefficients are calculated from the method proposed by Causone et al. [44]. The convective, radiative, and total heat transfer coefficients are computed from IAT, average unheated surface temperature (AUST) and OT, respectively.

The radiation heat transfer coefficient is calculated from the net radiation heat flux between the cooling surface and other surfaces using the equation (B.1) given below.

$$\frac{Qr}{A} = \sigma\Sigma_{j=1}^{n} F_{\epsilon_{s-j}}\left(T_s^4 - T_j^4\right) = h_r\left(AUST - T_s\right) \tag{B.1}$$

$$F_{\epsilon_{s-j}} = \frac{1}{\left[\frac{1-\epsilon_s}{\epsilon_s}\right] + \left(\frac{1}{F_{s-j}}\right) + \left(\frac{A_s}{A_j}\right)\left[\frac{1-\epsilon_s}{\epsilon_s}\right]} \tag{B.2}$$

The area-weighted surface temperature of non-radiant surfaces is considered to be the AUST [59]. The total heat transfer coefficient between the ceiling and indoor space is calculated from total heat flux using Eq. (B.3).

$$\frac{Q_{tot}}{A} = \frac{mc_p\Delta T_w}{A} - \frac{Q_{out}}{A} = h_{tot}\left(T_{op} - T_s\right) \tag{B.3}$$

The convective heat transfer coefficient is calculated from convective heat flux between the ceiling surface and indoor space (Eq. B.4).

$$\frac{Q_c}{A} = \frac{Q_{tot}}{A} - \frac{Q_r}{A} = h_c\left(T_a - T_s\right) \tag{B.4}$$

Where, A is the area (m^2), AUST is the average unheated surface temperature (°C), $c_p$is the specific heat (J/kgK), $F_{s_{s-j}}$ is the radiation interchange factor, h_c is the convective heat transfer coefficient (W/m^{2}K), h_r is the radiant heat transfer coefficient (W/m^{2}K), h_{tot} is the total heat transfer coefficient (W/m^{2}K), m is the mass flow rate (kg/s), Q_c is convective heat flux (W), Q_{out} is the backward heat transfer (W), Q_r is the radiant heat flux (W), Q_{tot} is the total heat flux (W), T_a is the air temperature (°C,)T_{mrt} is the mean radiant temperature (°C), T_{op} is the operative temperature (°C), T_r is the radiant surface temperature (°C), T_j is the j-surface temperature (°C), ΔT_w is the temperature difference between the water inlet and outlet (°C), and σ is the Stefan–Boltzmann constant (W m^{2}K^4). The convective, radiative, and total heat transfer coefficients obtained from the experimental studies are 4.0, 6.1, and 10.7 W/m^{2}K, respectively.

References

[1] IEO, in: International Energy Outlook 2017 Overview, U.S. Energy Information Administration IEO2017, 2017, p. 143. www.eia.gov/forecasts/ieo/pdf/0484(2016).pdf.

[2] M.V. Lucon, O. Ürge-Vorsatz, D. Ahmed, A.Z. Akbari, H. Bertoldi, P. Cabeza, L. F. Vilariño, Mitigation of climate change: contribution of working group III to the fourth assessment report of the intergovernmental panel on climate change, 2007.

[3] U.S. IEA, in: US Energy Information Administration, International Energy Outlook 2017 Overview, International Energy Outlook, IEO2017, 2017, p. 143. https://www.eia.gov/outlooks/ieo/pdf/0484(2017).pdf.

[4] A.K. Mishra, M. Ramgopal, An adaptive thermal comfort model for the tropical climatic regions of India (K??ppen climate type A), Build. Environ. 85 (2015) 134–143, doi:10.1016/j.buildenv.2014.12.006.

[5] D. Saelens, W. Parys, R. Baetens, Energy and comfort performance of thermally activated building systems including occupant behavior, Build. Environ. 46 (2011) 835–848, doi:10.1016/j.buildenv.2010.10.012.

[6] C. Stetiu, Energy and peak power savings potential of radiant cooling systems in US commercial buildings, Energy Build. 30 (1999) 127–138, doi:10.1016/S0378-7788(98)00080-2.

[7] D.O. Rijksen, C.J. Wisse, A.W.M. van Schijndel, Reducing peak requirements for cooling by using thermally activated building systems, Energy Build. 42 (2010) 298–304, doi:10.1016/j.enbuild.2009.09.007.

[8] M. Gwerder, B. Lehmann, J. Tödtli, V. Dorer, F. Renggli, Control of thermally-activated building systems (TABS), Appl. Energy 85 (2008) 565–581, doi:10.1016/j.apenergy.2007.08.001.

[9] D.G. Leo Samuel, S.M.S. Nagendra, M.P. Maiya, Feasibility analysis of passive thermally activated building system for various climatic regions in India, Energy Build. 155 (2017) 352–363, doi:10.1016/j.enbuild.2017.08.083.

[10] D.G. Leo Samuel, S.M.S. Nagendra, M.P. Maiya, Passive alternatives to mechanical air conditioning of building: a review, Build. Environ. 66 (2013) 54–64, doi:10.1016/j.buildenv.2013.04.016.

[11] P. Vangtook, S. Chirarattananon, Application of radiant cooling as a passive cooling option in hot humid climate, Build. Environ. 42 (2007) 543–556, doi:10.1016/j.buildenv.2005.09.014.

[12] X. Xu, S. Wang, J. Wang, F. Xiao, Active pipe-embedded structures in buildings for utilizing low-grade energy sources: a review, Energy Build. 42 (2010) 1567–1581, doi:10.1016/j.enbuild.2010.05.002.

[13] J. Feng, F. Bauman, Evaluation of cooling performance of thermally activated building system with evaporative cooling source for typical United States climates, Escholarsh, Univ. Calif. (2013).

[14] J. Feng, Design and Control of Hydronic Radiant Cooling Systems, Department of Architecture, University of California, Berkeley, 2014 (Ph.D. Dissertation) www.escholarship.org/uc/item/6qc4p0fr .

[15] Z. Tian, J.A. Love, A field study of occupant thermal comfort and thermal environments with radiant slab cooling, Build. Environ. 43 (2008) 1658–1670, doi:10.1016/j.buildenv.2007.10.012.

[16] B.W. Olesen, Using building mass to heat and cool, ASHRAE J. 54 (2012) 44–52.

[17] K.N. Rhee, B.W. Olesen, K.W. Kim, Ten questions about radiant heating and cooling systems, Build. Environ. 112 (2017) 367–381, doi:10.1016/j.buildenv.2016.11.030.

[18] M. Schmelas, T. Feldmann, P. Wellnitz, E. Bollin, Adaptive predictive control of thermo-active building systems (TABS) based on a multiple regression algorithm: first practical test, Energy Build. 129 (2016) 367–377, doi:10.1016/j.enbuild.2016.08.013.

[19] M. Pomianowski, P. Heiselberg, R.L. Jensen, Dynamic heat storage and cooling capacity of a concrete deck with PCM and thermally activated building system, Energy Build. 53 (2012) 96–107, doi:10.1016/j.enbuild.2012.07.007.
[20] A. Schlueter, A. Rysanek, F. Meggers, 3for2: realizing spatial, material, and energy savings through integrated design, CTBUH J. (2016) 40–45.
[21] K.W. Chen, E. Teitelbaum, F. Meggers, J. Pantelic, A. Rysanek, Exploring membrane-assisted radiant cooling for designing comfortable naturally ventilated spaces in the tropics, Build. Res. Inf. 0 (2020) 1–13, doi:10.1080/09613218.2020.1847025.
[22] E. Teitelbaum, K.W. Chen, D. Aviv, K. Bradford, L. Ruefenacht, D. Sheppard, M. Teitelbaum, F. Meggers, J. Pantelic, A. Rysanek, Membrane-assisted radiant cooling for expanding thermal comfort zones globally without air conditioning, Proc. Natl. Acad. Sci. U. S. A. 117 (2020) 21162–21169, doi:10.1073/pnas.2001678117.
[23] B. Ning, S. Schiavon, F.S. Bauman, A novel classification scheme for design and control of radiant system based on thermal response time, Energy Build. 137 (2017) 38–45, doi:10.1016/j.enbuild.2016.12.013.
[24] J. Romaní, A. De Gracia, L.F. Cabeza, Simulation and control of thermally activated building systems (TABS), Energy Build. 127 (2016) 22–42, doi:10.1016/j.enbuild.2016.05.057.
[25] Y.F. Wu, The structural behavior and design methodology for a new building system consisting of glass fiber reinforced gypsum panels, Constr. Build. Mater. 23 (2009) 2905–2913, doi:10.1016/j.conbuildmat.2009.02.026.
[26] K. Dharmasastha, S.M.S. Nagendra, M.P. Maiya, A numerical investigation of thermally activated glass fibre reinforced gypsum roof, in: Proceedings of the 24th National and 2nd International ISHMT-ASTFE Heat and Mass Transfer Conference, 2017.
[27] K.C.K. Vijaykumar, P.S.S. Srinivasan, S. Dhandapani, A performance of hollow clay tile (HCT) laid reinforced cement concrete (RCC) roof for tropical summer climates, Energy Build. 39 (2007) 886–892, doi:10.1016/j.enbuild.2006.05.009.
[28] P. Cherian, S. Paul, S.R.G. Krishna, D. Menon, A. Meher Prasad, Mass housing using GFRG panels: a sustainable, rapid and affordable solution, J. Inst. Eng. Ser. A 98 (2017) 95–100, doi:10.1007/s40030-017-0200-8.
[29] D. Menon, A.M. Prasad, GFRG/Rapidwall Building Structural Design Manual, Building Materials & Technology Promotion Council, Ministry of Housing & Urban Poverty Alleviation, Government of India, 2012.
[30] J. Romaní, L.F. Cabeza, G. Pérez, A.L. Pisello, A. de Gracia, Experimental testing of cooling internal loads with a radiant wall, Renew. Energy 116 (2018) 1–8, doi:10.1016/j.renene.2017.09.051.
[31] A. Frank, L. Wright, Radiant floor heating in theory and practice, ASHRAE J. 44 (7) (2002) 19–24.
[32] D. Saelens, W. Parys, R. Baetens, Energy and comfort performance of thermally activated building systems including occupant behavior, Build. Environ. 46 (2011) 835–848, doi:10.1016/j.buildenv.2010.10.012.
[33] E. Shaviv, A. Yezioro, I.G. Capeluto, Thermal mass and night ventilation as passive cooling design strategy, Renew. Energy 24 (3–4) (2001) 445–452.
[34] Y.W. Fung, W.L. Lee, Identifying the most influential parameter affecting natural ventilation performance in high-rise high-density residential buildings, Indoor Built Environ. 24 (2015) 803–812, doi:10.1177/1420326X14536189.
[35] S. Omrani, V. Garcia-Hansen, B.R. Capra, R. Drogemuller, Effect of natural ventilation mode on thermal comfort and ventilation performance: full-scale measurement, Energy Build. 156 (2017) 1–16, doi:10.1016/j.enbuild.2017.09.061.
[36] D.G. Leo Samuel, S.M.S. Nagendra, M.P. Maiya, Parametric analysis on the thermal comfort of a cooling tower based thermally activated building system in tropical climate – an experimental study, Appl. Therm. Eng. 138 (2018) 325–335, doi:10.1016/j.applthermaleng.2018.04.077.
[37] T. Kim, S. Kato, M. Shuzo, J.-W. Rho, Studyon indoor thermal environment of office space controlled by cooling panel system using field measurement and the numerical simulation, Building and Environment 40 (3) (2005) 301–310, doi:10.1016/j.buildenv.2004.04.010.
[38] K. Dharmasastha, S.M.S. Nagendra, M.P. Maiya, Performance study of thermally activated glass fibre reinforced gypsum roof, in: Int. High Perform. Build. Conf. Pap. 280, 2018: pp. 1–10. https://docs.lib.purdue.edu/ihpbc/280.
[39] K. Dharmasastha, D.G.L. Samuel, S.M.S. Nagendra, M.P. Maiya, Experimental investigation of thermally activated glass fibre reinforced gypsum roof, Energy Build. 228 (2020), doi:10.1016/j.enbuild.2020.110424.
[40] ASHRAE 55, Thermal environmental conditions for human occupancy, ASHRAE Inc. 2010 (2010) 42. ISSN 1041-2336.
[41] X. Zhai, Y. Li, X. Cheng, R. Wang, Experimental investigation on a solar-powered absorption radiant cooling system, Energy Procedia 70 (2015) 552–559, doi:10.1016/j.egypro.2015.02.160.
[42] W.H. Chiang, C.Y. Wang, J.S. Huang, Evaluation of cooling ceiling and mechanical ventilation systems on thermal comfort using CFD study in an office for subtropical region, Build. Environ. 48 (2012) 113–127, doi:10.1016/j.buildenv.2011.09.002.
[43] F. Nicol, M. Humphreys, Derivation of the adaptive equations for thermal comfort in free-running buildings in European standard EN15251, Build. Environ. 45 (2010) 11–17, doi:10.1016/j.buildenv.2008.12.013.
[44] F. Causone, S.P. Corgnati, M. Filippi, B.W. Olesen, Experimental evaluation of heat transfer coefficients between radiant ceiling and room, Energy Build. 41 (2009) 622–628, doi:10.1016/j.enbuild.2009.01.004.
[45] A.K. Mishra, M. Ramgopal, Field studies on human thermal comfort - an overview, Build. Environ. 64 (2013) 94–106, doi:10.1016/j.buildenv.2013.02.015.
[46] R.A. Memon, S. Chirarattananon, P. Vangtook, Thermal comfort assessment and application of radiant cooling: a case study, Build. Environ. 43 (2008) 1185–1196, doi:10.1016/j.buildenv.2006.04.025.
[47] M. Stevens, Human Body Heat as a Source for Thermoelectric Energy Generation, Stanford University Fall, 2016 Introd. to Phys. Energy2016.
[48] W. Jin, J. Ma, L. Jia, Z. Wang, Dynamic variation of surface temperatures on the radiant ceiling cooling panel based on the different supply water temperature adjustments, Sustain. Cities Soc. 52 (2020) 101805, doi:10.1016/j.scs.2019.101805.
[49] W. Zhao, S. Lestinen, S. Kilpeläinen, R. Kosonen, Comparison of the effects of symmetric and asymmetric heat load on indoor air quality and local thermal discomfort with diffuse ceiling ventilation, Int. J. Vent. 0 (2020) 1–16, doi:10.1080/14733315.2020.1839243.
[50] CEN, EN 16798-1 - Energy performance of buildings - Ventilation for buildings. Part 1: indoor environmental input parameters for design and assessment of energy performance of buildings addressing indoor air quality, thermal environment, lighting and acoustics, 2020.
[51] F. Tartarini, S. Schiavon, T. Cheung, T. Hoyt, CBE thermal comfort tool: online tool for thermal comfort calculations and visualizations, SoftwareX 12 (2020) 100563, doi:10.1016/j.softx.2020.100563.
[52] S. Silva, A. Monteiro, M.A. Russo, J. Valente, C. Alves, T. Nunes, C. Pio, A.I. Miranda, Modelling indoor air quality: validation and sensitivity, Air Qual. Atmos. Health 10 (2017) 643–652, doi:10.1007/s11869-016-0458-4.
[53] M. Mijakowski, J. Sowa, An attempt to improve indoor environment by installing humidity-sensitive air inlets in a naturally ventilated kindergarten building, Build. Environ. 111 (2017) 180–191, doi:10.1016/j.buildenv.2016.11.013.
[54] S.C. Lee, M. Chang, Indoor and outdoor air quality investigation at schools in Hong Kong, Chemosphere 41 (2000) 109–113, doi:10.1016/S0045-6535(99)00396-3.
[55] S. Gupta, M. Khare, R. Goyal, Sick building syndrome-a case study in a multistory centrally air-conditioned building in the Delhi City, Build. Environ. 42 (2007) 2797–2809, doi:10.1016/j.buildenv.2006.10.013.
[56] U. Satish, M.J. Mendell, K. Shekhar, T. Hotchi, D. Sullivan, Concentrations on human decision-making performance, Environ. Health Perspect. 120 (2012) 1671–1678.
[57] CENTechnical Report CR 1752: Ventilation for Buildings: Design Criteria for the Indoor Environment, European Committee for Standardization, Brussels, 1998.
[58] D. Kumar, D.G. Leo Samuel, S.M. Shiva, N. Maiya, M. Prakash, Influence of natural ventilation and indoor heat load on radiant ceiling cooling system, Mendeley Data V1 (2022), doi:10.17632/kpns2mnw2p.1.
[59] ASHRAE HVAC Systems and Equipment HandbookChapter 6: Panel Heating and Cooling, American Society of Heating Refrigeration and Air-conditioning Engineers, USA, 2000.